IEEE Access
Multidisciplinary | Rapid Review | Open Access Journal

Received July 2, 2018, accepted August 10, 2018, date of publication August 22, 2018, date of current version October 8, 2018.

Digital Object Identifier 10.1109/ACCESS.2018.2866601

An Approach for Noninvasive Blood Glucose Monitoring Based on Bioimpedance Difference Considering Blood Volume Pulsation

JINGZHEN LI[1], TOBORE IGBE[1,2], YUHANG LIU[1], ZEDONG NIE[1], (Member, IEEE), WENJIAN QIN[1], LEI WANG[1], (Member, IEEE), AND YANG HAO[3], (Fellow, IEEE)

[1]Shenzhen Institutes of Advanced Technology, Chinese Academy of Sciences, Shenzhen 518055, China
[2]Graduate University of Chinese Academy of Sciences, Beijing 100049, China
[3]School of Electronic Engineering and Computer Science, Queen Mary University of London, London E1 4NS, U.K.

Corresponding author: Zedong Nie (zd.nie@siat.ac.cn)

This work was supported in part by the National Natural Science Foundation of China under Grant 61871375 and Grant U1505251, in part by the Guangdong Science and Technology Plan Project under Grant 2015B020233004, and in part by the Shenzhen Public Technology Service Platform Improvement Project of Biomedical Electronics.

ABSTRACT Noninvasive blood glucose monitoring (NBGM) provides a promising solution for patients with diabetes with the advantages of painless and continuous monitoring. To better characterize the response of glucose to radio-frequency (RF) signals at low frequencies, the conductivity and relative permittivity of aqueous solutions with different glucose concentrations were obtained by the use of an impedance analyzer in the frequency range of 1 kHz to 1 MHz. Furthermore, considering the blood volume pulsation in cardiac cycle, a new approach based on measuring bioimpedance was presented for NBGM in this paper. For this purpose, an inhomogeneous arm model, which consists of three tissue layers (i.e., blood, blood vessel, and other relevant tissues), was proposed to validate the aforementioned approach. Furthermore, the measurements were carried out by means of *in vitro* experiment and *in vivo* studies, respectively. The results showed that as the glucose concentration increased, the conductivity of aqueous solutions decreased when the frequency of RF signal was below 1 MHz. However, the relative permittivity was almost insensitive to glucose concentration. The simulation result of the arm model showed that as the glucose concentration increased, the bioimpedance difference of blood volume decreased. This was supported by both *in vitro* and *in vivo* experiments. We therefore suggest that the proposed approach for NBGM has potentials in practical applications.

INDEX TERMS Bioimpedance, blood volume pulsation, dielectric properties, digital phantoms, *in vitro* and *in vivo* experiments, noninvasive blood glucose monitoring (NBGM).

I. INTRODUCTION

Diabetes, which is characterized as hyperglycemia, is a worldwide epidemic disease [1]. The number of patients with diabetes, as estimated by International Diabetes Federation (IDF), is expected to increase from 425 million in 2017 to 629 million by 2045. Furthermore, four million deaths happened as a result of diabetes and its complications, and the global healthcare costs which was dedicated to diabetes treatment and related complication reached 727 billion dollar in 2017 [2]. Currently, to avoid diabetic complications such as kidney failure, diabetic retinopathy and neuropathy, maintenance of blood glucose concentration within the physiological range through antidiabetic drugs is of great importance. Therefore, the frequent monitoring of blood glucose is an essential part of diabetic management [3]. Generally, the patients need to withdraw blood from the finger with a lancet, and the glucose level is acquired by blood strip [4]. However, frequent finger pricks can become quite painful if a regular monitoring is needed. In other words, the aforementioned approach is invasive and is not suited for continuous monitoring of blood glucose.

Over the last few decades, the noninvasive blood glucose monitoring (NBGM) technology has been introduced due to the advantages of being painless and suitable for continuous monitoring [5]–[7]. Based on the technologies being employed, NBGM can usually be categorized as optical

monitoring and non-optical monitoring [8]–[10]. Thus far, many researchers have tried to demonstrate the feasibility of different optical monitoring technologies, involving near infrared spectroscopy [11], [12], mid-infrared spectroscopy [13], Raman spectroscopy [14], optical rotation of polarized light [15], optical coherence tomography [16], and so on. Meanwhile, a limited number of studies have been published utilizing non-optical techniques for sensing the changes of blood glucose concentration. Karacolak *et al.* [17] performed measurements on blood samples collected from different volunteers. Specifically, the correlation between dielectric properties (*i.e.*, relative permittivity and conductivity) of blood plasma and glucose concentration was measured by using the vector network analyzer at a frequency range of 500 MHz to 20 GHz. Furthermore, the Cole-Cole equation of blood plasma with eight different glucose concentrations was derived from fitting. Similarly, the relative permittivity and conductivity of the blood samples with different glucose concentrations were acquired over a frequency range of 1 GHz to 10 GHz in [18]. In [19], the blood mimicking phantoms with four different glucose concentrations were fabricated, and the dielectric properties of blood mimicking phantoms were investigated in the frequency range of 300 MHz to 20 GHz. The aqueous solutions with glucose concentrations of 100 mg/dL to 500 mg/dL were used as the experimental subject in [20], and the dielectric properties of aqueous solutions were measured in the frequency range of 1 GHz to 8 GHz. In addition, the S11 and S21 parameters of aqueous solutions with different glucose concentrations were studied using a transmission/ reflection line approach with a frequency range between 100 MHz and 4 GHz in [21]. The results indicated that the S21 parameter was easily affected by noise. In [22] and [23], a microwave sensor, which was comprised of two spatially separated split-ring resonators, operating at approximately 1.43 GHz, was proposed for NBGM on volunteers with and without diabetes. The resonant frequency of S21 and its 3-dB bandwidth were obtained by the use of a network analyzer. In [24], a miniature spiral sensor was adopted for NBGM. Moreover, the S11 was investigated at different glucose concentrations when the frequency was between 3 GHz and 7 GHz. In addition, a microstrip spiral resonator was proposed for blood glucose monitoring in [25] and [26], and the S parameters were measured by *in vitro* or i*n vivo* studies. To sum up, the aforementioned investigations were mainly focused on the dielectric properties of different glucose concentrations and the S parameters (S11 or S21) of sensing signals in relation to the changes of glucose concentration in the blood sample at high radio-frequency (RF)/microwave frequencies (hundreds of MHz or even GHz). On the other hand, according to Schwan's dispersion theory, the biological tissue shows α dispersion and β dispersion at low frequencies (under dozens of MHz) [27]. Therefore, it may be inferred that the sensing signal is equally sensitive to the glucose concentration at lower frequencies. However, thus far, very few investigations have been reported. In [28], the impedance spectroscopies of aqueous solutions with different glucose concentrations were measured in the frequency range 50 Hz to 1 MHz. Additionally, the impact of temperature on impedance spectroscopies of different glucose concentrations was explored at frequencies from 100 kHz to 10 MHz in [29]. Furthermore, as is well known, the blood volume in the blood vessel presents a cyclical change when the blood flows, owing to the periodic pulsation of the heart [30]. Specifically, blood volume is largest when the heart is in the systolic state, and it is smallest when the heart is in the diastolic state. Therefore, it may lead to periodical variations of NBGM data due to the blood volume pulsation at each cardiac cycle. However, the influence of blood volume pulsation on NBGM was neglected in aforementioned previous studies.

In this paper, dielectric properties of aqueous solutions with different glucose concentrations will be investigated in the frequency range from 1 kHz to 1 MHz. Additionally, taking into account the blood volume pulsation in a full cardiac cycle, an approach based on measuring bioimpedance difference is proposed for NBGM. Firstly, the bioimpedance of a forearm at each cardiac cycle is measured by the polygraph system with the sampling rate of 1000 Hz. Subsequently, the difference between minimum and maximum bioimpedance values at each cardiac cycle is obtained. Secondly, the bioimpedance variation associated with the change of blood glucose concentration will be investigated. We intend to decouple the influence of blood volume pulsation and other tissues (skin, fat, muscle, and so on) on glucose measurements by means of bioimpedance subtraction.

The remainder of this paper is organized as follows. In Section II, we will demonstrate the dielectric properties of aqueous solutions with ten different glucose concentrations and the fitting result. In Section III, in order to validate the feasibility of the new approach, an inhomogeneous arm model will be established, and the influence of glucose concentrations on bioimpedance difference will be studied. Section IV and Section V will present *in vitro* and *in vivo* measurement results, respectively. Finally, the conclusions are drawn in Section VI.

II. DIELECTRIC PROPERTIES

A. DIELECTRIC PROPERTIES OF AQUEOUS SOLUTIONS WITH DIFFERENT GLUCOSE CONCENTRATIONS

In order to more intuitively understand the influence of glucose concentration on dielectric properties at low frequencies, higher glucose concentrations were taken into account in this paper. Thus, the glucose concentrations considered in this work are not representative of the blood glucose concentrations in humans. Specifically, the value of the glucose concentrations in this paper was varied from 0 mmol/L to 225 mmol/L, and the difference between adjacent concentrations was 25 mmol/L. As shown in Fig. 1, the relative permittivity and conductivity of aqueous solutions with different glucose concentrations were measured by the impedance analyzer (E4990A, Keysight) and liquid test

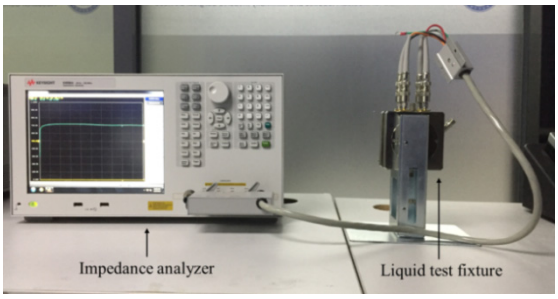

FIGURE 1. Measurement of dielectric properties of aqueous solutions with different glucose concentrations by using impedance analyzer and liquid test fixture.

fixture (16452A, Keysight) in the frequency range between 1 kHz and 1 MHz. The measurement routine of each aqueous solution sample was repeated three times, and 1,200 data points were collected at each time. The room temperature was 24°C during the measurements.

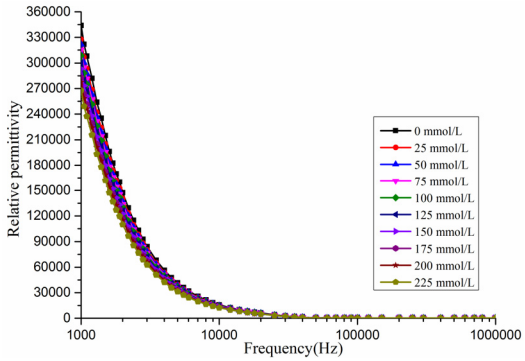

FIGURE 2. Relative permittivity of aqueous solutions with different glucose concentrations between 1 kHz to 1 MHz.

Fig. 2 demonstrates the relative permittivity of aqueous solutions with different glucose concentrations in the frequency range between 1 kHz and 1 MHz. It could be observed that the relative permittivity of all aqueous solutions decreased sharply against the frequency when it was below 10 kHz. For instance, the relative permittivity was more than 270,000 at the frequency of 1 kHz, whereas the value was approximately 12,000 at 10 kHz, less than 350 at 100 kHz. However, on the other hand, the difference of relative permittivity of aqueous solutions with different glucose concentrations was not obvious in the whole frequency range. What is more, the difference became smaller when the frequency was more than 100 kHz. Therefore, our measurements indicated that the relative permittivity was almost insensitive to the glucose concentrations.

Fig. 3 illustrates the conductivity of aqueous solutions with different glucose concentrations. With respect to frequency, the conductivity increased sharply below 10 kHz. Subsequently, the conductivity increased slowly between 10 kHz and 1 MHz. As illustrated in Fig. 3, it is interesting to observe that the conductivity of aqueous solutions was

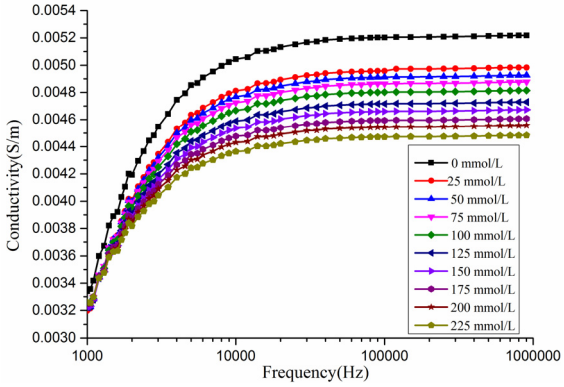

FIGURE 3. Conductivity of aqueous solutions with different glucose concentrations from 1 kHz to 1 MHz.

closely related to glucose concentration. As the glucose concentration increased, the conductivity decreased. For example, the conductivity was 0.005202 S/m, 0.004801 S/m, and 0.004471 S/m at 25 kHz when the glucose concentrations were chosen at 0 mmol/L, 100mmol/L, and 225mmol/L, respectively.

B. FITTING PARAMETERS OF DIFFERENT GLUCOSE CONCENTRATIONS

As reported in [31], the Cole–Cole equation could be used to describe the dielectric properties of biological tissues. The Cole–Cole equation of three poles is listed as (1). Moreover, the imaginary part of Cole-Cole equation is associated with the conductivity of biological tissues, as shown in (2) [32]. Therefore, the conductivity could be obtained through (3). Please note that the distribution parameter α of Cole–Cole equation was set as 0 in our work. In this paper, to better evaluate the influence of glucose concentration on conductivity, equation (3) was used to describe the measured conductivity of different aqueous solutions as a function of frequency. As listed in (3), ε_0 is the permittivity of free space and its value is 8.854×10^{-12} F/m; $\Delta\varepsilon_1$, $\Delta\varepsilon_2$, $\Delta\varepsilon_3$ are the difference of relative permittivity; τ_1, τ_2, τ_3 represent the relaxation time of blood samples; f is the signal frequency, and σ_0 is the static conductivity. Fig. 4 shows the fitting result by means of (3) when the glucose concentration was 0 mmol/L. In addition, the fitting parameters of conductivity of aqueous solutions with different glucose concentrations are listed in Table 1.

$$\hat{\varepsilon}(f) = \varepsilon'(f) - j\varepsilon''(f) = \varepsilon_\infty + \sum_{n=1}^{3} \frac{\Delta\varepsilon_n}{1 + j2\pi f \tau_n^{(1-\alpha_n)}} + \frac{\sigma_0}{j2\pi f \varepsilon_0} \tag{1}$$

$$\varepsilon''(f) = \frac{\sigma(f)}{2\pi f \varepsilon_0} \tag{2}$$

$$\sigma(f) = \left(\frac{2\pi \cdot f \cdot \Delta\varepsilon_1 \cdot \tau_1}{1 + (2\pi \cdot f \cdot \tau_1)^2} + \frac{2\pi \cdot f \cdot \Delta\varepsilon_2 \cdot \tau_2}{1 + (2\pi \cdot f \cdot \tau_2)^2} + \frac{2\pi \cdot f \cdot \Delta\varepsilon_3 \cdot \tau_3}{1 + (2\pi \cdot f \cdot \tau_3)^2} + , \frac{\sigma_0}{2\pi \cdot f \cdot \varepsilon_0}\right) \cdot 2\pi \cdot f \cdot \varepsilon_0 \tag{3}$$

TABLE 1. The fitting parameters of conductivity of aqueous solutions with different glucose concentrations.

glucose (mmol/L)	$\Delta\varepsilon_1$	τ_1 (s)	$\Delta\varepsilon_2$ (s)	τ_2 (s)	$\Delta\varepsilon_3$	τ_3 (s)	σ_0 (S/m)
0	88.14	7.43548×10^{-6}	1621.66	3.86768×10^{-5}	47139.27	1.46005×10^{-4}	0.00188
25	82.50	7.23555×10^{-6}	1531.23	3.83768×10^{-5}	44344.33	1.50483×10^{-4}	0.00191
50	78.97	7.18041×10^{-6}	1450.85	3.81146×10^{-5}	43832.01	1.52846×10^{-4}	0.00195
75	76.28	7.1758×10^{-6}	1398.27	3.80639×10^{-5}	42815.69	1.54022×10^{-4}	0.00199
100	73.87	7.1611×10^{-6}	1347.48	3.79873×10^{-5}	41818.08	1.54997×10^{-4}	0.00201
125	69.83	7.10185×10^{-6}	1263.78	3.77238×10^{-5}	40571.92	1.5672×10^{-4}	0.00205
150	67.30	7.06424×10^{-6}	1212.09	3.75592×10^{-5}	39564.33	1.57849×10^{-4}	0.00208
175	63.67	7.00852×10^{-6}	1139.48	3.72452×10^{-5}	37894.95	1.60129×10^{-4}	0.00215
200	61.53	6.97485×10^{-6}	1094.99	3.70994×10^{-5}	37051.43	1.60976×10^{-4}	0.00217
225	58.09	6.92489×10^{-6}	1023.07	3.68094×10^{-5}	35420.94	1.62717×10^{-4}	0.00223

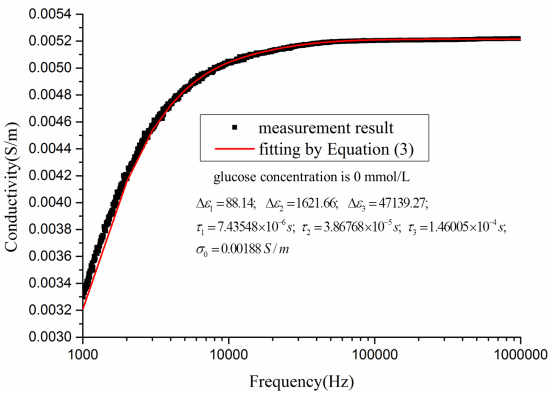

FIGURE 4. Fitting result of conductivity when the glucose concentration was 0 mmol/L in the frequency range between 1 kHz and 1 MHz.

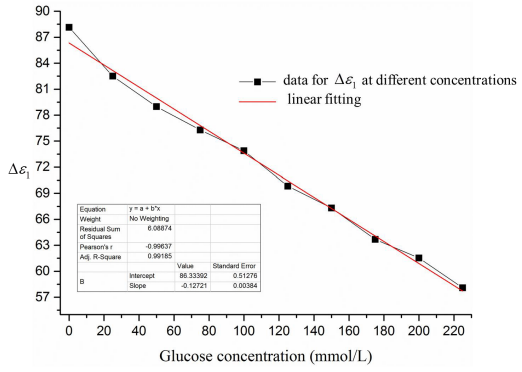

FIGURE 5. Linear fitting to the $\Delta\varepsilon_1$ variable with glucose concentrations.

An example of $\Delta\varepsilon_1$ variable with glucose concentrations is plotted in Fig. 5. It could be observed that $\Delta\varepsilon_1$ was almost linearly decreased as the glucose concentration increased. The other fitting parameters such as $\Delta\varepsilon_2$, $\Delta\varepsilon_3$, τ_1, and τ_2 also showed the similar variation. Therefore, the correlation between fitting parameters and glucose concentration could be approximately concluded with (4) to (10).

$$\Delta\varepsilon_1 = -0.12721 \cdot x + 86.3339 \tag{4}$$
$$\Delta\varepsilon_2 = -2.5794 \cdot x + 1598.477 \tag{5}$$
$$\Delta\varepsilon_3 = -47.806 \cdot x + 46423.50 \tag{6}$$
$$\tau_1 = -1.86026 \times 10^{-9} \cdot x + 7.3355 \times 10^{-6} \tag{7}$$
$$\tau_2 = -7.72679 \times 10^{-9} \cdot x + 3.8635 \times 10^{-5} \tag{8}$$
$$\tau_3 = 6.62977 \times 10^{-8} \cdot x + 1.48216 \times 10^{-4} \tag{9}$$
$$\sigma_0 = 1.52242 \times 10^{-6} \cdot x + 1.870 \times 10^{-3} \tag{10}$$

Where x is the glucose concentration (unit: mmol/L) of aqueous solutions.

III. BIOIMPEDANCE MODEL OF BLOOD GLUCOSE

A. BIOIMPEDANCE DIFFERENCE OF BLOOD VOLUME

Bioimpedance is the electrical impedance that is described by the complex relation between voltage and current when a voltage is applied across any biological tissue, and a current will tend to traverse the tissue. Considering that the bioimpedance of the human body is mainly controlled by the lean-tissue component, the bioimpedance can be written as (11) [33].

$$Z = \frac{L}{\sigma A} \tag{11}$$

where L is the length, A is the cross-sectional area, and σ is the conductivity of biological tissue.

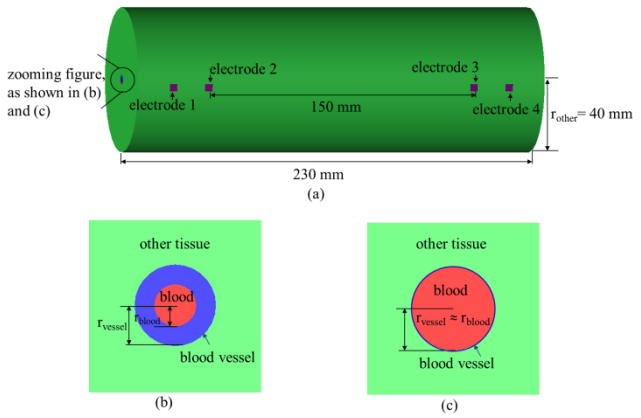

FIGURE 6. (a) Structure of inhomogeneous arm model proposed in this paper and the electrode position; (b) the cross-section of inhomogeneous arm model when the heart was in a diastolic state; (c) the cross-section of inhomogeneous arm model when the heart was in a systolic state.

In this section, an inhomogeneous arm model was proposed to evaluate the feasibility of measuring blood glucose concentrations based on the change of their bioimpedance. As described in Fig. 6, the arm model was comprised of three

major tissues, which were blood, blood vessels, and other relevant tissues, respectively. Four electrodes were attached on the arm surface. The current was injected into the arm model through electrode 1 and electrode 4. Additionally, a separate set of monitoring electrodes (electrode 2 and electrode 3) was used to measure the voltage developed across the arm model, and then the bioimpedance would be obtained. As is well known, the blood volume in the blood vessel and the thickness of blood vessel are consistently changing owing to the systolic and diastolic function of heart at a cardiac cycle [34]. In addition, the blood vessel is always filled with blood [35]. Therefore, as demonstrated in Fig. 6(b), in order to simplify the proposed model, we assumed that the thickness of blood vessel was largest when the heart was in a diastolic state. Similarly, as shown in Fig. 6(c), the thickness of blood vessel was smallest which was close to 0 mm when the heart was in a systolic state. At this moment, the blood volume was largest. According to (11), the bioimpedance of three tissues could be written as (12)-(14). Considering that three tissues were placed in parallel in the arm model, the total impedance of arm model could be acquired as (15).

$$Z_{blood} = \frac{L}{\pi \cdot \sigma_{blood} \cdot r_{blood}^2} \tag{12}$$

$$Z_{vessel} = \frac{L}{\pi \cdot \sigma_{vessel} \cdot (r_{vessel}^2 - r_{blood}^2)} \tag{13}$$

$$Z_{other} = \frac{L}{\pi \cdot \sigma_{other} \cdot (r_{other}^2 - r_{vessel}^2)} \tag{14}$$

$$Z_{total} = \frac{Z_{blood} \cdot Z_{vessel} \cdot Z_{other}}{Z_{blood} \cdot Z_{vessel} + Z_{blood} \cdot Z_{other} + Z_{vessel} \cdot Z_{other}} \tag{15}$$

Where σ_{blood}, σ_{vessel}, σ_{other} represent the conductivity of blood, blood vessel, and other relevant tissues, r_{blood}, r_{vessel}, r_{other} are the radius of blood volume, blood vessel, and other relevant tissues, respectively. L is the distance between electrode 2 and electrode 3.

As shown in (15), the bioimpedance of the arm model can be regarded as a combination of two types of impedances: 1) base impedance Z_{other}, which is corresponding to static tissues, such as muscle, bone and fat; 2) variable impedance of Z_{blood} and Z_{vessel}, which is corresponding to time-varying blood volume.

As described in Fig. 6 (b) and Fig. 6 (c), it is worth noting that the range of the radius of blood volume was set from 1.372 mm to 2.672 mm in this section, which was similar to [30] and [36]. The others parameters are listed as Table 2. Fig. 7 demonstrates the normalized bioimpedance as a function of the radius of blood volume when the glucose concentration was 100 mmol/L. As shown in Fig. 7, the radius of blood volume had a great impact on the bioimpedance. The bioimpedance of arm model was 1.0 Ω when the radius of blood volume was 1.372 mm. As the radius increased, the bioimpedance was almost linearly decreased. The bioimpedance was 0.997 Ω at the radius of 2.672 mm.

TABLE 2. The parameters of arm model in Fig. 6.

L (mm)	r_{other} (mm)	r_{vessel_min} (mm)	r_{vessel_max} (mm)	σ_{vessel} (S/m)	σ_{other} (S/m)
150	40	1.372	2.672	0.00234	0.00255

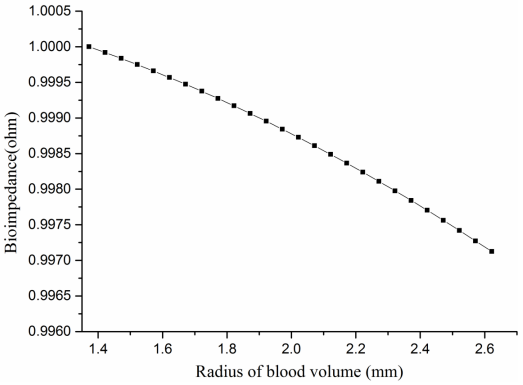

FIGURE 7. Bioimpedance of arm model various with the radius of blood volume.

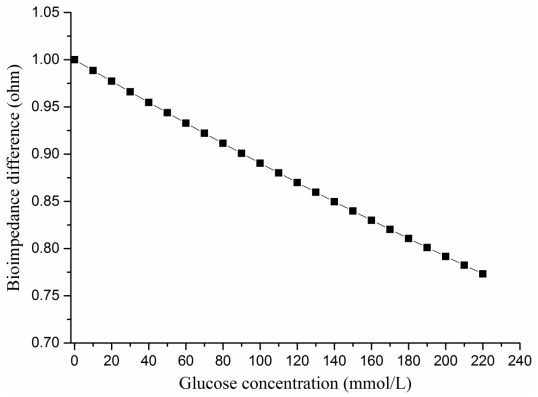

FIGURE 8. Bioimpedance difference varies with different glucose concentrations in arm model.

Fig. 8 illustrates the normalized bioimpedance difference when the glucose concentration is varied from 0 mmol/L to 225 mmol/L. The bioimpedance difference was 1.0 Ω when the glucose concentration was at 0 mmol/L. Furthermore, it could be observed that the bioimpedance difference was linearly decreased as the glucose concentration increased. The bioimpedance difference was 0.773 Ω at 220 mmol/L. Thus, it suggests that the glucose concentration can be obtained by measuring the change in bioimpedance.

B. CURRENT DENSITY DISTRIBUTION IN BIOIMPEDANCE MEASUREMENT

In this section, the current density distribution of arm model was explored by using commercial electromagnetic modeling software XFDTD which is based on the finite-difference time-domain (FDTD) method. Fig. 9 demonstrates the current density distribution of blood and blood vessel when the

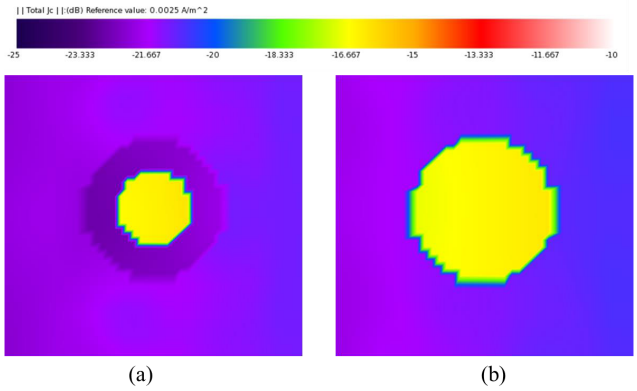

FIGURE 9. Current density distribution of blood and blood vessel at different radius of blood volume: (a) the heart was in a diastolic state and the radius of blood volume was 1.372 mm; (b) the heart was in a systolic state and the radius of blood volume was 2.672 mm.

radius of blood volume is 1.372 mm and 2.672 mm, respectively. The glucose concentration was set as 225 mmol/L. The reference value of current density was 0.0025 A/m^2 (*i.e.*, 0 dB). As shown in Fig. 9 (a), the current density of blood was about −16.45 dB, whereas the current density of blood vessel was less than −22.38 dB. In addition, the current density of interface between blood vessel and other relevant tissues was −18.33 dB. As the radius of blood volume increased, the thickness of blood vessel decreased. As shown in Fig.9 (b), the current density was approximately −16.43 dB in the blood and blood vessel. In other words, as the radius of blood volume increased, more current was injected into the arm model. Therefore, it could be inferred that the bioimpedance between electrode 2 and electrode 3 would be decreased, which corresponded with Fig. 7.

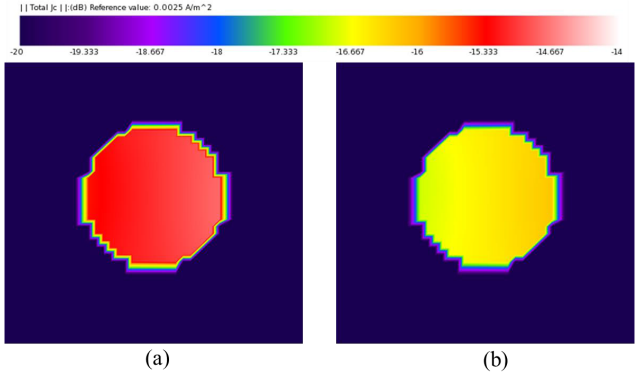

FIGURE 10. Current density distribution of blood and blood vessel at different glucose concentrations when the radius of blood volume was 2.672 mm: (a) the blood glucose concentration was 0 mmol/L; (b) the blood glucose concentration was 225 mmol/L.

Fig. 10 describes the current density distribution of blood and blood vessel at different glucose concentrations. The reference value of current density was also set as 0.0025 A/m^2 (*i.e.*, 0dB). The current density was from −15.35 dB to −14.82 dB in Fig. 10 (a) when the glucose concentration was 0 mmol/L. On the other hand, as shown in Fig. 10 (b), the current density was from −16.80 dB to −16.26 dB when the glucose concentration was at 225 mmol/L. Therefore, it indicated that the current density distribution was associated with the glucose concentration.

IV. IN VITRO MEASUREMENT OF BIOIMPEDANCE

A. IN VITRO EXPERIMENT SETUP

As illustrated in Fig. 11, to verify the feasibility of the proposed approach, an *in vitro* experiment was carried out by using the agar phantom. Specifically, the agar phantom, of which the dimension was 400 mm × 130 mm × 130mm, mimicked all relevant tissues. There was a hole of 350 mm × 110 mm × 55 mm in the agar phantom which represented the blood vessel. Please note that the dimension of agar phantom and its hole presented in this section are not the same with the arm model shown in Fig. 6, as its dimensions are very small and it was rather difficult to simulate. The aqueous solutions of 400 mL and 800 mL were poured into the hole respectively to mimic the change of blood volume due to the beating of heart. The experimental setup was as follows. Firstly, when the glucose concentration was set at 0 mmol/L, the bioimpedance of phantom with 400 mL and 800 mL aqueous solutions was measured respectively by using the polygraph system (model number: MP150 and EBI100C, Biopac). The EBI 100C can incorporate a precision current source of 100 uA rms. The operational frequency of 25 kHz was selected in this experiment. Subsequently, the bioimpedance difference between 400 mL and 800 mL could be obtained. Similarly, the bioimpedance difference was acquired when the glucose concentrations were 50 mmol/L, 100 mmol/L, 200 mmol/L, individually.

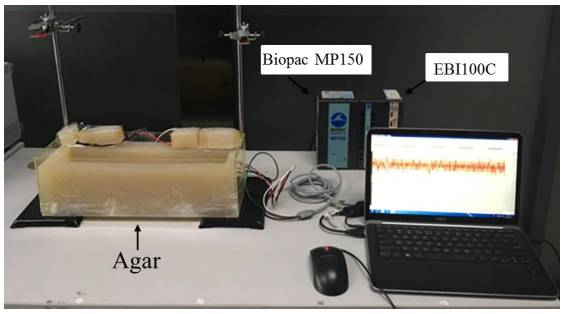

FIGURE 11. *In vitro* experiment setup.

B. IN VITRO MEASUREMENT RESULT

Fig. 12 shows the normalized bioimpedance difference as a function of glucose concentration *in vitro* experiment. The bioimpedance difference was 1.0 Ω, 0.964 Ω, 0.959 Ω, and 0.930 Ω when the glucose concentrations were 0 mmol/L, 50 mmol/L, 100 mmol/L, and 200 mmol/L, respectively. Thus, our *in vitro* measurement results supported the hypothesis that as the glucose concentration increases, the bioimpedance difference will decrease, which is very consistent with the trend presented in Fig. 8.

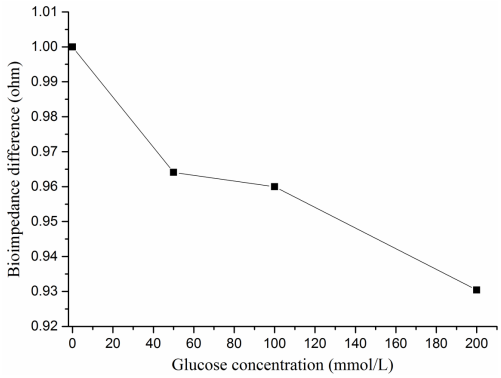

FIGURE 12. Bioimpedance difference various with the glucose concentration *in vitro* experiment.

V. *IN VIVO* MEASUREMENT OF BIOIMPEDANCE

A. IN VIVO EXPERIMENT SETUP

As shown in Fig. 13, the *in vivo* measurement was carried out on a nondiabetic volunteer. The volunteer was fasting more than 8 hours. The experiment began at 9:00am in the laboratory. Fifteen minutes later, the volunteer drank 65g glucose. The experiment continued for 135 minutes. The bioimpedance of volunteer's forearm was measured by using the polygraph system (model number: MP150 and EBI100C, Biopac). The frequency of current source in EBI100C was selected as 25 kHz and the amplitude was 100 uA rms. Four electrodes were attached on the surface of volunteer's arm, and the distance between electrode 2 and electrode 3 was 150 mm. The bioimpedance of arm at each cardiac cycle was collected by the software AcqKnowledge 4.2 which was provided by Biopac Systems, *inc.* Taking into account that the frequency of cardiac cycle is usually from 0.7 Hz to 3 Hz, the sampling rate of bioimpedance was set as 1000 Hz in this paper, which was sufficient to meet the requirements of bioimpedance measurement of arm at each cardiac cycle. Simultaneously, the blood glucose concentration of volunteer at different time was obtained from a commercial portable blood glucose meter and lancing device (model number: ACCU-CHEK® Performa meter).

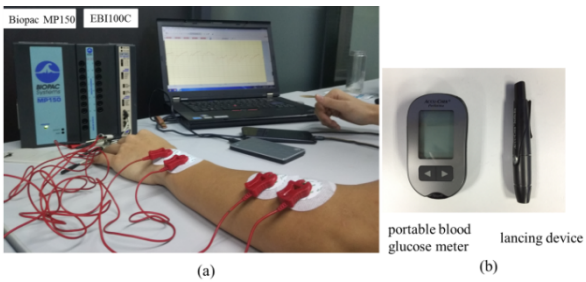

FIGURE 13. *In vivo* experiment setup: (a) the bioimpedance of arm was measured by using the polygraph system; (b) the blood glucose concentration of volunteer was acquired from the blood glucose meter and lancing device.

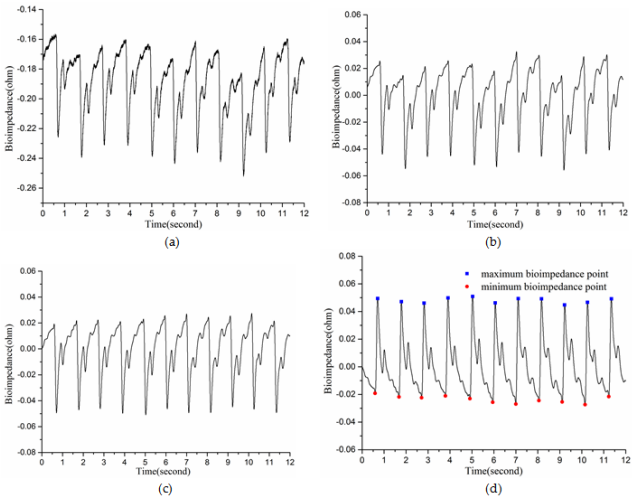

FIGURE 14. (a) Raw signal collected by the polygraph system; (b) the signal was processed by low pass filtered and high pass filtered; (c) the signal was processed by wavelets; (d) the maximum bioimpedance (solid square) and minimum bioimpedance (solid circle) was acquired at each cardiac cycle.

B. BIOIMPEDANCE EXTRACTION

The raw data collected by the polygraph system is plotted in Fig. 14(a). It could be observed that the measured signal is not clean owing to the influence of noise. Therefore, the data preprocessing is important before bioimpedance extraction. Fig. 15 shows the flow diagram of signal preprocessing and bioimpedance extraction. Specifically, a low pass filter with cut-off frequency of 10 Hz and a high pass filter with cut-off frequency of 0.2 Hz were utilized in this paper. As demonstrated in Fig. 14(b), the high frequency noise has been effectively filtered out. However, the signals were still fluctuating, which might be caused by human breathing. To remove its effect, the wavelet transform was adopted for signal preprocessing, as listed in (16), (17) and (18), which were implemented in the MATLAB.

$$[C,L] = \text{wavedec}(\text{original\_data}, 10, \text{'db10'}) \quad (16)$$

$$\text{noise} = \text{wrcoef}(\text{'a'}, C, L, \text{'db10'}, 10) \quad (17)$$

$$\text{wavelet\_data} = \text{original\_data} - \text{noise} \quad (18)$$

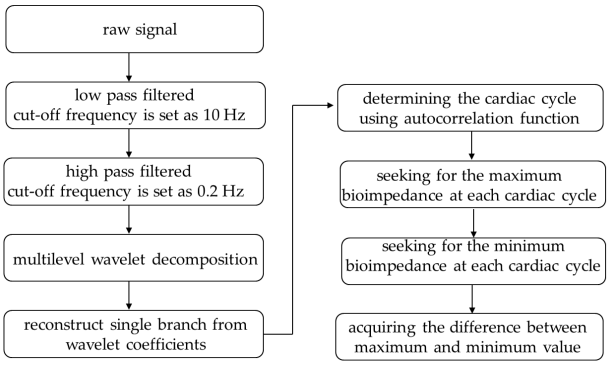

FIGURE 15. Flow diagram of bioimpedance extraction.

As listed in (16), the dataset was undergone wavelet decomposition at level 10 using the wavelet 'db10'. Then the coefficients were reconstructed based on the wavelet decomposition structure [C, L] at level 10. Finally, the measurement noise was effectively filtered out, as shown in Fig. 14(c).

The cardiac cycle was determined by using autocorrelation function in this paper. In addition, the maximum bioimpedance at each cardiac cycle was acquired by the finding peak function in MATLAB. The minimum bioimpedance at each cardiac cycle also could be obtained, as shown in Fig. 14(d). Please note that the signals in Fig. 14 (d) were inverted from Fig. 14(c). Finally, the bioimpedance difference between maximum and minimum for each cardiac cycle could be computed.

C. IN VIVO MEASUREMENT RESULT

The bioimpedance difference at each cardiac cycle collected over 5 minutes was averaged in this work. Fig. 16 shows the *in vivo* measurement result of a volunteer without diabetes, plotted as a function of time and compared with the reference blood glucose concentration. As shown in Fig. 16, the bioimpedance difference was about 0.6782 Ω when the volunteer was fasting and the blood glucose concentration was 4.8 mmol/L. The glucose intake was conducted at t = 15 minute. The bioimpedance difference was 0.5860 Ω at t = 30 minute. Furthermore, the bioimpedance difference was 0.6372 Ω at t = 65 minute, and the blood glucose concentration was approximately 7.3 mmol/L. Subsequently, the bioimpedance difference increased to 0.7446 Ω at t = 70 minute. At that moment, the blood glucose concentration showed a downward trend. The bioimpedance difference was 0.7306 Ω and blood glucose concentration was 5.6 mmol/L at t = 135 minute. On the other hand, in terms of the variety of blood glucose concentration, it could be fitted as (19), which is quadratic polynomial. Similarly, the change of bioimpedance difference could be fitted as (20). As shown in Fig. 16, the opening direction of fitting curve about blood glucose concentration was downward, whereas the opening direction of fitting curve about bioimpedance difference was upward, which corresponded with the trend in Fig. 8 and Fig. 12.

$$\Delta\rho_{glu\cos e} = -5.635 \times 10^{-4} \cdot t^2 + 0.0829 \cdot t + 4.265 \quad (19)$$

$$\Delta Z = -1.478 \times 10^{-6} \cdot t^2 - 1.594 \times 10^{-4} \cdot t + 0.0732 \quad (20)$$

Where $\Delta\rho_{glu\cos e}$ represents the blood glucose concentration (unit: mmol/L), ΔZ represents the bioimpedance difference (unit: Ω), and t is time (unit: minute).

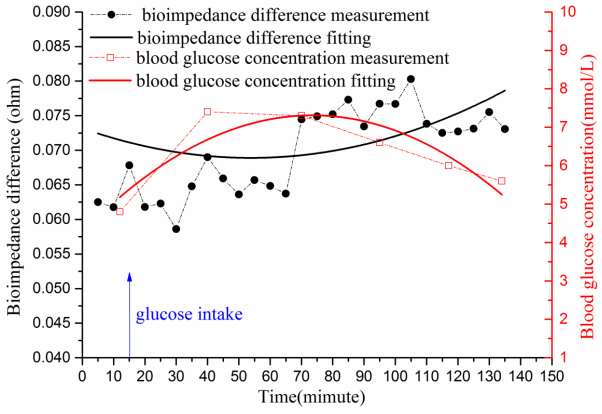

FIGURE 16. Bioimpedance difference and the blood glucose concentration *in vivo* experiment.

D. DISCUSSION

As shown in Fig. 8, the result of arm model showed that as the glucose concentration increased, the bioimpedance difference decreased. Furthermore, the result of *in vitro* experiment in Fig. 12 also demonstrated the same trend that the bioimpedance difference decreased with the increasing of glucose concentration. In addition, the result of *in vivo* experiment in Fig. 16 showed the similar trend to Fig. 8 and Fig. 12. For instance, the bioimpedance difference was 0.06593 Ω at t = 45 minute, and the blood glucose concentration was about 7.4 mmol/L. Subsequently, as blood glucose was decomposed, the blood glucose concentration presented a decreasing trend. The blood glucose concentration was 6.6 mmol/L at t = 95 minute. It could be observed that the as the blood glucose concentration decreased, the bioimpedance difference showed an increased trend that the bioimpedance difference had been increased from 0.06593 Ω to 0.07672 Ω at 45 ≤ t ≤ 95 minute. However, there were still some unsatisfied results in Fig. 16. Specifically, the blood glucose concentration was the smallest at t ≤ 15 minute while the volunteer was fasting. After the glucose intake, the blood glucose centration began to increase. Thus, according to the inference of Fig. 8 and Fig. 12, the bioimpedance difference of fasting state at t ≤ 15 minute in Fig. 16 should be the larger than the bioimpedance difference after glucose intake. However, the bioimpedance difference was similar between fasting state and after glucose intake in Fig. 16. In other words, it was indicated that there was a deviation of bioimpedance difference at t ≤ 15 minute. The deviation in Fig. 16 might be explained as follows. Firstly, the deviation was caused by the temperature difference between the human and electrodes at t ≤ 15 minute. The temperature of human body was about 37°C, whereas the electrode temperature was room temperature, which was 24°C. As reported in [22] and [29], the temperature might have an impact on NBGM. Secondly, both the maximum blood volume and minimum blood volume were set as a constant in arm model and *in vitro* experiment. However, in fact, the maximum blood volume at each cardiac cycle has little fluctuation, and so does the minimum blood volume. The instability of maximum blood volume and minimum blood volume *in vivo* experiment might lead to the deviation of bioimpedance difference. Furthermore, the components of blood are very complicated, including blood glucose, hemoglobin, inorganic substance, and so on. The changes of other components of blood also

may cause the deviation of bioimpedance measurement on NBGM. Thirdly, the electrode polarization at low frequencies might have an impact on the bioimpedance measurement, which would lead to the deviation in Fig. 16 [37], [38].

On the other hand, measurement of bioimpedance requires the injection of an electric current. Therefore, no harm or disturbance of any kind should happen to biological tissue. In this paper, the frequency and amplitude of injected current was below the threshold strength-duration curve of the excitable tissues, so it would not elicit the harm or disturbance of tissue [39]. However, the possible implication of running current through the body for long-term bioimpedance measurement still needs to be studied.

VI. CONCLUSIONS

In this paper, the relative permittivity and conductivity of aqueous solutions with ten different glucose concentrations were measured in the frequency range of 1 kHz to 1 MHz. The result showed that the relative permittivity was almost insensitive to glucose concentrations. However, as the glucose concentration increased, the conductivity decreased. The conductivity dropped from 0.00520 S/m to 0.00447 S/m at 25 kHz when the glucose concentration was from 0 mmol/L to 225 mmol/L. In addition, a new approach based on measuring bioimpedance was presented for NBGM. To verify the feasibility of aforementioned approach, an inhomogeneous arm model was established in this paper. The simulation result indicated that the normalized bioimpedance difference would fall from 1.0 Ω to 0.773 Ω when the glucose concentration increased from 0 mmol/L to 225 mmol/L. Furthermore, the *in vitro* experiment with an agar phantom and *in vivo* experiment with a nondiabetic volunteer were carried out in this paper. The normalized bioimpedance difference *in vitro* experiment was 1.0 Ω, 0.964 Ω, 0.959 Ω, and 0.930 Ω when the glucose concentrations were 0 mmol/L, 50 mmol/L, 100 mmol/L, and 200 mmol/L, respectively, which was consistent with the variety trend of the arm model. Additionally, the *in vivo* experiment also showed the similar trend at $t \geq 15$ minute. Therefore, it might be concluded that the approach based on bioimpedance difference was feasible for NBGM. In the near future, we will conduct more *in vivo* studies via different volunteers (diabetic patients and normal people). In addition, we will investigate bioimpedance measurement based on multi-frequency, which may be of help to decouple the influence of other components of blood on NBGM.

ACKNOWLEDGMENT

(Jingzhen Li and Tobore Igbe contributed equally to this work.)

REFERENCES

[1] E. Öztürk, A. K. K. Arslan, M. B. Yerer, and A. Bishayee, "Resveratrol and diabetes: A critical review of clinical studies," *Biomed. Pharmacotherapy*, vol. 95, pp. 230–234, Nov. 2017.

[2] *IDF Diabetes Atlas*, 8th ed., Int. Diabetes Fed., Brussels, Belgium, 2017. [Online]. Available: http://www.diabetesatlas.org

[3] J. Y. Lucisano, T. L. Routh, J. T. Lin, and D. A. Gough, "Glucose monitoring in individuals with diabetes using a long-term implanted sensor/telemetry system and model," *IEEE Trans. Biomed. Eng.*, vol. 64, no. 9, pp. 1982–1993, Sep. 2017.

[4] C. Chen, X.-L. Zhao, Z.-H. Li, Z.-G. Zhu, S.-H. Qian, and A. J. Flewitt, "Current and emerging technology for continuous glucose monitoring," *Sensors*, vol. 17, no. 1, p. 182, Jan. 2017.

[5] N. A. B. A. Salam, W. H. bin Mohd Saad, Z. B. Manap, and F. Salehuddin, "The evolution of non-invasive blood glucose monitoring system for personal application," *J. Inst. Electron. Telecommun. Eng.*, vol. 8, no. 1, pp. 59–65, Jan. 2016.

[6] A. Facchinetti, "Continuous glucose monitoring sensors: Past, present and future algorithmic challenges," *Sensors*, vol. 16, no. 12, p. E2093, Dec. 2016.

[7] H. Ali, F. Bensaali, and F. Jaber, "Novel approach to non-invasive blood glucose monitoring based on transmittance and refraction of visible laser light," *IEEE Access*, vol. 5, pp. 9163–9174, May 2017.

[8] J. Yadav, A. Rani, V. Singh, and B. M. Murari, "Prospects and limitations of non-invasive blood glucose monitoring using near-infrared spectroscopy," *Biomed. Signal Process. Control*, vol. 18, pp. 214–227, Apr. 2015.

[9] O. Cherkasova, M. Nazarov, and A. Shkurinov, "Noninvasive blood glucose monitoring in the terahertz frequency range," *Opt. Quantum Electron.*, vol. 48, p. 217, Mar. 2016.

[10] J. Kottmann, J. M. Rey, and M. W. Sigrist, "Mid-infrared photoacoustic detection of glucose in human skin: Towards non-invasive diagnostics," *Sensors*, vol. 16, no. 10, p. E1663, Oct. 2016.

[11] X. F. Lu, T. L. Zhang, F. Xiao, G. Li, and Y. Wang, "Noninvasive blood glucose analysis based on near-infrared reflectance spectroscopy," *Spectrosc. Spectr. Anal.*, vol. 36, no. 7, pp. 2312–2317, Jul. 2016.

[12] M. Goodarzi, S. Sharma, H. Ramon, and W. Saeys, "Multivariate calibration of NIR spectroscopic sensors for continuous glucose monitoring," *TrAC Trends Anal. Chem.*, vol. 67, pp. 147–158, Apr. 2015.

[13] S. Liakat, K. A. Bors, L. Xu, C. M. Woods, J. Doyle, and C. F. Gmachl, "Noninvasive *in vivo* glucose sensing on human subjects using mid-infrared light," *Biomed. Opt. Express*, vol. 5, no. 7, pp. 2397–2404, Jul. 2014.

[14] W. C. Shih, K. L. Bechtel, and M. V. Rebec, "Noninvasive glucose sensing by transcutaneous Raman spectroscopy," *J. Biomed. Opt.*, vol. 20, no. 5, p. 051036, May 2015.

[15] N. Ozana *et al.*, "Noncontact speckle-based optical sensor for detection of glucose concentration using magneto-optic effect," *J. Biomed. Opt.*, vol. 21, no. 6, p. 065001, Jun. 2016.

[16] L. R. De Pretto, T. M. Yoshimura, M. S. Ribeiro, and A. Z. de Freitas, "Optical coherence tomography for blood glucose monitoring *in vitro* through spatial and temporal approaches," *J. Biomed. Opt.*, vol. 21, no. 8, p. 086007, Aug. 2016.

[17] T. Karacolak, E. C. Moreland, and E. Topsakal, "Cole–cole model for glucose-dependent dielectric properties of blood plasma for continuous glucose monitoring," *Microw. Opt. Technol. Lett.*, vol. 55, no. 5, pp. 1160–1164, Mar. 2013.

[18] J. Venkataraman and B. Freer, "Feasibility of non-invasive blood glucose monitoring: *In-vitro* measurements and phantom models," in *Proc. IEEE Int. Symp. Antennas Propag. (APSURSI)*, Washington, DC, USA, Jul. 2011, pp. 603–606.

[19] T. Yilmaz, R. Foster, and Y. Hao, "Broadband tissue mimicking phantoms and a patch resonator for evaluating noninvasive monitoring of blood glucose levels," *IEEE Trans. Antennas Propag.*, vol. 62, no. 6, pp. 3064–3075, Jun. 2014.

[20] V. Turgul and I. Kale, "Characterization of the complex permittivity of glucose/water solutions for noninvasive RF/microwave blood glucose sensing," in *Proc. IEEE Int. Instrum. Meas. Technol. Conf.*, Taiwan, China, May 2016, pp. 1–5.

[21] C. G. Juan, E. Bronchalo, G. Torregrosa, E. Ávila, N. García, and J. M. Sabater-Navarro, "Dielectric characterization of water glucose solutions using a transmission/reflection line method," *Biomed. Signal Process. Control*, vol. 31, pp. 139–147, Jan. 2017.

[22] H. Choi *et al.*, "Design and *in vitro* interference test of microwave noninvasive blood glucose monitoring sensor," *IEEE Trans. Microw. Theory Techn.*, vol. 63, no. 10, pp. 3016–3025, Oct. 2015.

[23] H. Choi, S. Luzio, J. Beutler, and A. Porch, "Microwave noninvasive blood glucose monitoring sensor: Human clinical trial results," in *IEEE MTT-S Int. Microw. Symp. Dig.*, Honolulu, HI, USA, Jun. 2017, pp. 876–879.

[24] J. Shao, F. Yang, F. Xia, Q. Zhang, and Y. Chen, "A novel miniature spiral sensor for non-invasive blood glucose monitoring," in *Proc. 10th Eur. Conf. Antennas Propag. (EuCAP)*, Davos, Switzerland, 2016, pp. 1–2.
[25] T. Yilmaz, R. Foster, and Y. Hao, "Towards accurate dielectric property retrieval of biological tissues for blood glucose monitoring," *IEEE Trans. Microw. Theory Techn.*, vol. 62, no. 12, pp. 3193–3204, Dec. 2014.
[26] R. J. Buford, E. C. Green, and M. J. Mcclung, "A microwave frequency sensor for non-invasive blood-glucose measurement," in *Proc. IEEE Sensors Appl. Symp.*, Atlanta, GA, USA, Feb. 2008, pp. 4–7.
[27] H. P. Schwan, "Analysis of dielectric data: Experience gained with biological materials," *IEEE Trans. Electr. Insul.*, vol. EI-20, no. 6, pp. 913–922, Dec. 1985.
[28] J. Juansah and W. Yulianti, "Studies on electrical behavior of glucose using impedance spectroscopy," in *Proc. IOP Conf. Ser., Earth Environ. Sci.*, Bogor, Indonesia, 2016, p. 012039.
[29] S. Sbrignadello, A. Tura, and P. Ravazzani, "Electroimpedance spectroscopy for the measurement of the dielectric properties of sodium chloride solutions at different glucose concentrations," *J. Spectrosc.*, vol. 2013, Jul. 2013, Art. no. 571372.
[30] S. Laurent *et al.*, "Elastic modulus of the radial artery wall material is not increased in patients with essential hypertension," *Arteriosclerosis Thrombosis, J. Vascular Biol.*, vol. 14, no. 7, pp. 1223–1231, Jul. 1994.
[31] S. Gabriel, R. W. Lau, and C. Gabriel, "The dielectric properties of biological tissues: III. Parametric models for the dielectric spectrum of tissues," *Phys. Med. Biol.*, vol. 41, no. 11, pp. 2271–2293, Apr. 1996.
[32] C. Gabriel, S. Gabriel, and E. Corthout, "The dielectric properties of biological tissues: I. Literature survey," *Phys. Med. Biol.*, vol. 41, no. 11, pp. 2231–2249, Apr. 1996.
[33] M. E. Valentinuzzi, J. P. Morucci, and C. J. Felice, "Bioelectrical impedance techniques in medicine. Part II: Monitoring of physiological events by impedance," *Crit. Rev. Biomed. Eng.*, vol. 24, nos. 4–6, pp. 353–466, 1996.
[34] T. Iijima *et al.*, "Cardiac output and circulating blood volume analysis by pulse dye-densitometry," *J. Clin. Monit.*, vol. 13, no. 2, pp. 81–89, Mar. 1997.
[35] J. Mayet and A. Hughes, "Cardiac and vascular pathophysiology in hypertension," *Heart*, vol. 89, no. 9, pp. 1104–1109, 2003.
[36] T. Ashraf, Z. Panhwar, S. Habib, M. A. Memon, F. Shamsi, and J. Arif, "Size of radial and ulnar artery in local population," *J. Pakistan Med. Assoc.*, vol. 60, no. 10, pp. 817–819, Oct. 2010.
[37] P. B. Ishai, M. S. Talary, A. Caduff, E. Levy, and Y. Feldman, "Electrode polarization in dielectric measurements: A review," *Meas. Sci. Technol.*, vol. 24, no. 10, pp. 102001–102021, Oct. 2013.
[38] A. Caduff, M. S. Talary, and Y. Feldman, "Comment on experimental methods and conclusions of impedance spectroscopy of solutions at physiological glucose concentrations by A. Tura, S. Sbrignadello, S. Barison, S. Conti, G. Pacini," *Biophys. Chem.*, vol. 132, no. 2, pp. 165–166, Feb. 2008.
[39] M. E. Valentinuzzi, "Bioelectrical impedance techniques in medicine. Part I: Bioimpedance measurement. First section: General concepts," *Crit. Rev. Biomed. Eng.*, vol. 24, nos. 4–6, pp. 223–255, 1996.

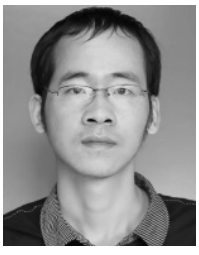

JINGZHEN LI received the B.E. and M.Sc. degrees from the College of Electronic Science and Technology, Shenzhen University, Shenzhen, China, in 2011 and 2014, respectively.

He is currently a Research Assistant with the Shenzhen Institutes of Advanced Technology, Chinese Academy of Sciences. His research interests include body sensor network and blood glucose monitoring.

TOBORE IGBE received the B.Tech. and M.Tech. degrees from the Federal University of Technology at Akure, Akure, Nigeria, in 2010 and 2015, respectively.

He is currently pursuing the Ph.D. degree with the Center of Medical Robotics and Minimal Invasive Surgical Devices Center, Shenzhen Institutes of Advanced Technology, Chinese Academy of Sciences. His research interests include machine learning, data mining, computer vision, and imaging analysis.

YUHANG LIU received the B.Sc. and M.Sc. degrees from Yunnan University, Kunming, China, in 2012 and 2015, respectively.

She is currently a Research Assistant with the Shenzhen Institutes of Advanced Technology, Chinese Academy of Sciences. Her research interests include human body communication for body sensor network, electromagnetic fields, and magnetic waves.

ZEDONG NIE received the M.Sc. degree from the Wuhan University of Science and Technology, Wuhan, China, in 2007, and the Ph.D. degree from the University of Chinese Academy of Sciences, Beijing, China, in 2013.

Since 2013, he has been an Associate Professor with the Shenzhen Institutes of Advanced Technology, Chinese Academy of Sciences. His current research interests include short range communication, wearable technology, body sensor network, and medical electronics.

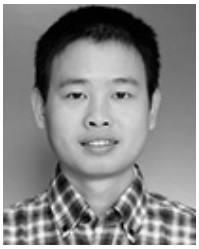

WENJIAN QIN received the B.S. degree from Shenyang Aerospace University in 2009 and the M.S. degree from the University of Chinese Academy Sciences in 2012. From 2016 to 2017, he was a Visiting Scholar with the Laboratory of Artificial Intelligence in Medicine and Biomedical Physics, Stanford University. He is currently a Research Assistant with the Shenzhen Institutes of Advanced Technology, Chinese Academy of Sciences.

His research interests include computer vision, machine learning, and biomedical imaging analysis.

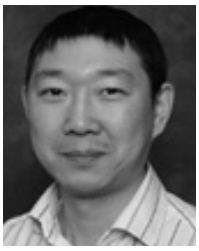

LEI WANG received the B.S. degree in information and control engineering and the Ph.D. degree in biomedical engineering from Xi'an Jiaotong University, China, in 1995 and 2000, respectively. Subsequently, he took various research roles at different U.K. universities.

From 2001 to 2008, he was with the University of Glasgow, Glasgow, U.K., and Imperial College London, London, U.K. He is currently with the Shenzhen Institutes of Advanced Technology, Chinese Academy of Sciences, Shenzhen, China, as a Professor and the Deputy Director with the Institute of Biomedical and Health Engineering. He has authored more than 200 scientific papers, nine books/book chapters, and filed 60 patents. His research interests focus on body sensor networks.

YANG HAO (M'00–SM'06–F'13) received the Ph.D. degree in electrical and electronic engineering from the Centre for Communications Research, University of Bristol, Bristol, U.K., in 1998. He is currently a Professor of antennas and electromagnetics with the Antenna Engineering Group, Queen Mary University of London, London, U.K. Prior to his appointment at the Queen Mary University of London, he was a Post-Doctoral Research Fellow with the School of Electronic, Electrical and Computer Engineering, University of Birmingham, Birmingham, U.K. Over the years, he developed several fully integrated antenna solutions based on novel artificial materials to reduce mutual RF interference, weight, cost, and system complexity for security, aerospace, and healthcare. He developed, with leading U.K. industries, novel and emergent gradient index materials to reduce mass, footprint, and profile of low-frequency and broadband antennas. He coined the term body-centric wireless communications, i.e., networking among wearable and implantable wireless sensors on the human body. He was the first to characterize and include the human body as a communication medium between on-body sensors using surface and creeping waves. He contributed to the industrial development of the first wireless sensors for healthcare monitoring. He is also a strategic advisory board member for the Engineering and Physical Sciences Research Council, where he is committed to championing RF/microwave engineering for reshaping the future of U.K. manufacturing and electronics. He has published over 140 journal papers.

Prof. Hao was elected as a fellow of the ERA Foundation in 2007 and a fellow of IET in 2010. He is currently an Editor-in-Chief of the IEEE Antennas and Propagation Letters. He was an Associate Editor of the same journal and of the IEEE Transactions on Antennas and Propagation from 2008 to 2013 and also a Co-Guest Editor for the IEEE Transactions on Antennas and Propagation in 2009.